Distinct Exciton Dissociation Behavior of Organolead Trihalide Perovskite and Excitonic Semiconductors Studied in the Same System

Miao Hu, Cheng Bi, Yongbo Yuan, Zhengguo Xiao, Qingfeng Dong, Yuchuan Shao, and Jinsong Huang*

Organolead trihalide perovskites ($CH_3NH_3PbX_3$; X is Cl, Br, I, or a combination of them, $MAPbX_3$) are organic/inorganic hybrid materials with a very strong absorption in the ultraviolet–visible (UV–vis) range comparable to the best organic photovoltaic (OPV) materials. From "dye" in dye sensitized solar cells (DSSC),[1] to "hole conductors"[2] and "electron conductors"[3] in mesoscopic heterojunction solar cells, there has been a dramatic conceptual evolution on the function of $MAPbI_3$ in photovoltaic devices. Recently, planer heterojunction (PHJ) perovskite solar cells were demonstrated to have an efficiency comparable with mesoporous structure devices.[4] This raises a fundamental question: whether the organic–inorganic hybrid perovskites are excitonic or nonexcitonic semiconductors. In excitonic semiconductors incident photons generate tightly bound charge pairs, while free charges in nonexcitonic semiconductors because of the large difference in exciton binding energies between them, namely, Frenkel excitons or Mott–Wannier excitons. The reported exciton binding energy, which distinguishes excitonic and nonexcitonic semiconductors, has a large variation from 19 to 56 meV.[5] Despite the large variation, the exciton binding energy of $MAPbI_3$ is larger than that of III–V inorganic semiconductors with the same bandgap, while being significantly smaller than that of most organic semiconductors, generally in the range of 0.2–1.0 eV.[6] Though not conclusive yet, some recent work has shown the differences in perovskite with conventional excitonic materials. Bisquert and co-workers observed the charge accumulation in $MAPbI_3$ in mesoporous solar cells, inferring that $MAPbX_3$ constitutes a new kind of photovoltaic material different from dyes in DSSC.[7] Recently, D'Innocenzo et al. demonstrated that there is almost a full ionization of the exciton population in $MAPbX_3$ under photovoltaic cell operating conditions by the temperature dependent optical absorption and numerical simulation of the ratio of free charges to excitons.[8] The results

implied a nonexcitonic character for $MAPbX_3$, but did not offer direct evidence for the difference between organolead trihalide perovskites and excitonic materials. A more clear recognition of excitonic nature processed by this material system is required to further understand the operation mechanism of this new type of photovoltaic device, which potentially can provide a guidance to further optimize the device structure for improving the device efficiency.

In this study, we show the direct evidence for the nonexcitonic nature of organolead trihalide perovskites by comparing the exciton dissociation behavior of perovskites to conventional excitonic semiconductors in the same device. The open circuit voltage (V_{OC}) output in the perovskite devices is found to be independent of the lowest unoccupied molecular orbital (LUMO) of the "acceptors." From the incident photon to charge carrier efficiency (IPCE) study, we observe that the excitons could get a maximum dissociation in perovskite without any external field or a heterogeneous interface acting on it, while exciton dissociation in excitonic semiconductor materials was strongly field dependent. The results indicate that $MAPbX_3$ photovoltaic cells should be treated as traditional inorganic thin film photovoltaic devices, rather than organic or hybrid ones.

We first examined the dielectric constant of the $MAPbI_3$ thin films with impedance spectroscopy. The low dielectric screening is the origin of large exciton binding energy in organic semiconductors, making it excitonic in nature. Surprisingly, the dielectric constant of $MAPbI_3$ was barely studied until recently, which might be due to the difficulty to form the pin–hole free perovskite thin films. The recent study of dielectric response of $MAPbI_3$ was executed on the devices containing multiple layers including mesoporous or compact electrodes,[9] thus did not measure the dielectric property of the perovskite layer itself exclusively. In this study, we apply a recently developed interdiffusion approach to form the continuous, leakage-free perovskite thin films.[4] This pin–hole free 1 μm $MAPbI_3$ film, whose surface and cross section scanning electron microscope images are shown in **Figure 1**a,b, gives us the opportunity to study the dielectric properties of this single layer material. The perovskite films were deposited on poly(3,4-ethylenedioxythiophene):poly(4-styrenesulfonate) PEDOT:PSS covered indium tin oxide (ITO) or bare ITO substrates, and were covered by gold electrodes with a simple

M. Hu, C. Bi, Dr. Y. Yuan, Z. Xiao, Q. Dong, Y. Shao, Prof. J. Huang
Department of Mechanical and Materials Engineering and Nebraska Center for Materials and Nanoscience
University of Nebraska–Lincoln
Lincoln, NE 68588–0526, USA
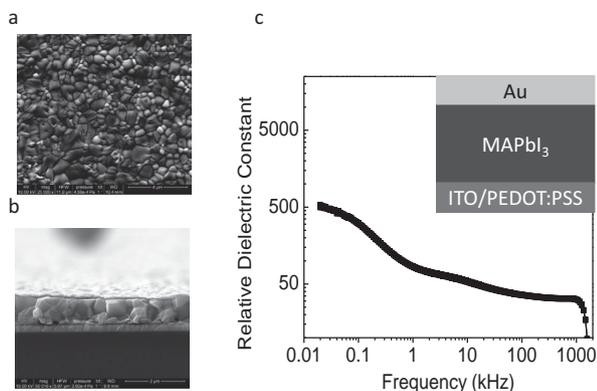E-mail: jhuang2@unl.edu

Figure 1. Top view a) and cross-section view b) of the scan electron microscope images of the $MAPbI_3$ film fabricated by interdiffusion method. c) Frequency-dependent relative dielectric constant of the $MAPbI_3$ film. The $MAPbI_3$ film based device structure for dielectric constant measurement is shown in the inset.

device structure as shown in the inset of Figure 1c. The frequency dependent dielectric constant of the devices was measured in dark condition at zero bias to avoid any poling effect. A giant dielectric constant over 500 was observed on a low frequency of 20 Hz, which is lower than the dark dielectric constant of >1000 reported by Bisquert and co-workers.[9] The discrepancy can be explained by the different material fabrication method used because charge trapping and detrapping in the nanocrystalline TiO_2 film can cause huge dielectric response in the low frequency range. This also indicates the importance to differentiate the dielectric response from that of other layers using a single layer perovskite film. As we can see, the relative dielectric constant is about 32 at high frequencies,

in consistent with that measured by Poglitsch and Weber with a dispersive polarizing millimeter-wave interferometer.[10] Such a large relative dielectric constant indicates that $MAPbI_3$ is a nonexcitonic material, as the Coulomb interaction between electron and hole pairs can be effectively screened.

Next, we examined the variation of V_{OC} of the $MAPbI_3$ devices with different fullerenes as electron extraction layers to find out whether the LUMO level of fullerenes determines the V_{OC} of the $MAPbI_3$ devices. A signature of OPVs is that their V_{OC} is determined by the energy level difference between the LUMO of the acceptor and the highest occupied molecular orbital (HOMO) of the donor. Fullerenes (including their derivatives) were first introduced to PHJ perovskite solar cells as electron acceptors and later used to produce high efficiency devices.[11] The initial study of fullerenes employed PHJ perovskite solar cell by Jeng et al. showed the V_{OC} of the device with different fullerenes was well correlated with the LUMO of fullerenes,[11] leading one to wonder whether perovskite solar cell devices work in a mechanism similar to OPVs. It was recently demonstrated by us that the variation of V_{OC} should be caused by the Schottky junction formed between the different fullerenes with PEDOT:PSS because the formed perovskite films from premixed precursor solution were actually discontinuous, resulting in a direct contact of fullerenes with PEDOT:PSS.[12] The continuous, pin–hole free perovskite films formed by the interdiffusion method again allow us to conclusively study the influence of LUMO levels of fullerenes on the device V_{OC} output. The fullerene and its derivatives, including C_{60}, [6,6]-phenyl C_{61}-butyric acid methyl ester (PCBM), indene-C_{60} bi-adduct (ICBA), indene-C_{60} tri-adducts (ICTA), which have a large LUMO variation of 0.97 eV (**Figure 2**), were used in
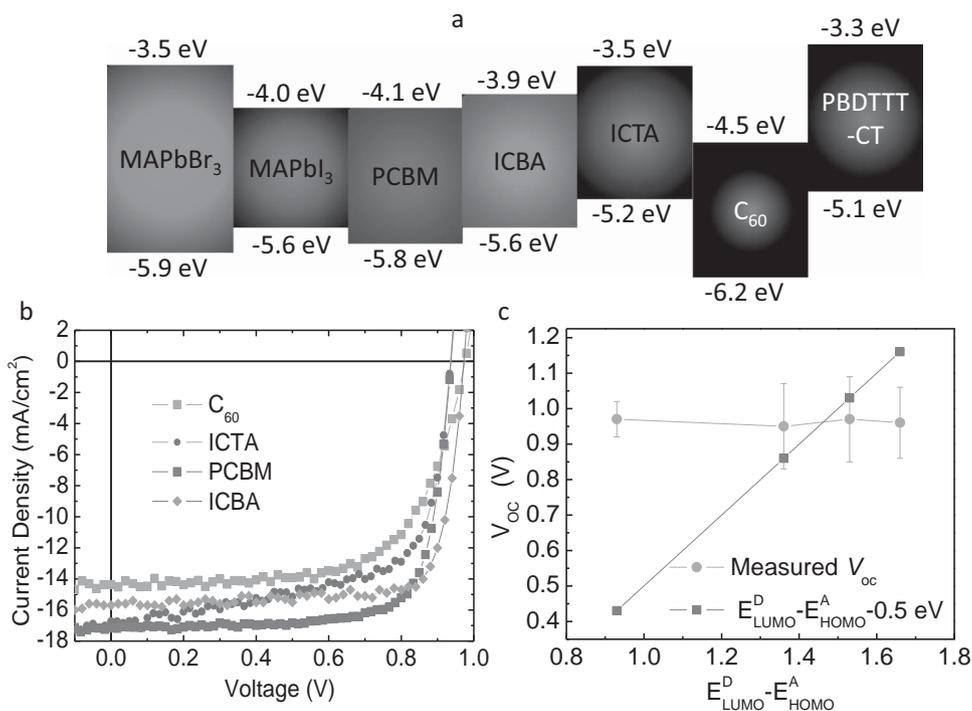

Figure 2. a) Energy levels of $MAPbI_3$, $MAPbBr_3$, various fullerenes, and PBDTTT-CT. b) Photocurrent curves of $MAPbI_3$ photovoltaic devices with varied fullerene layers. c) Correlation of V_{oc} of the devices and the offset between the LUMO of $MAPbI_3$ and the HOMOs of fullerenes.
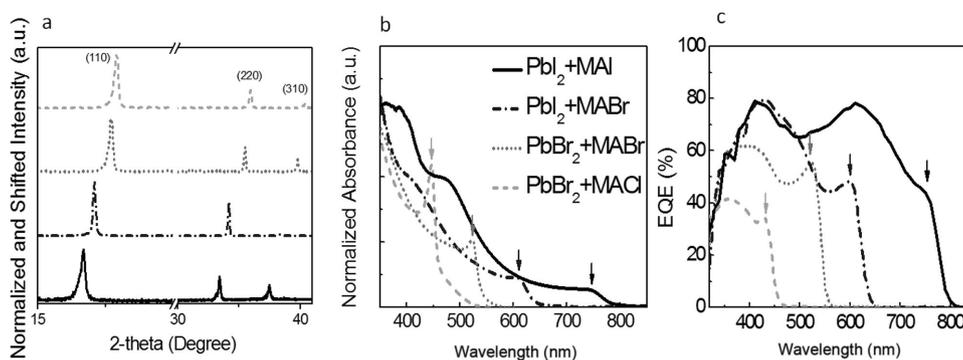
Figure 3. a) X-ray diffraction patterns of perovskite films fabricated from varied precursors. b) Normalized absorption spectra of the corresponding perovskite films. c) EQE spectra of devices built on the corresponding perovskite films.

the following regular PHJ device structure: ITO/PEDOT:PSS/MAPbI$_3$/spun fullerenes/C$_{60}$/2,9-dimethyl-4,7-diphenyl-1,10-phenanthroline (BCP)/Al. Data in Figure 2b,c clearly show that the V_{OC} of MAPbI$_3$ solar cells is independent of the LUMO of the fullerenes, in striking contrast to the rule in OPVs where eV_{OC} = LUMO(A)-HOMO(D)-0.5 eV.[13,14] Thus we can conclude that the fullerenes in MAPbI$_3$ based PHJ solar cells mainly work as electron transport layers rather than electron acceptors in OPVs.[15] Another fact supporting this conclusion is that the LUMO level of ICTA is higher than the conduction band (CB) bottom of MAPbI$_3$, while the device with ICTA still works efficiently. It has also been demonstrated that changing the hole extraction layer could not alter the V_{OC} as well.[14] The fact that the V_{OC} of MAPbI$_3$ solar cells is exclusively dominated by the perovskite layer itself, rather than by the electron or hole collection layers if there is absence of Fermi energy pinning effect; this provides further evidence that MAPbI$_3$ is a nonexcitonic semiconductor.

We then studied the exciton generation and dissociation in organolead bromide and organolead bromide-chloride mixed halide perovskites, which might have a larger exciton binding energy due to a larger bandgap. Here, we formed the organolead mixed halide perovskite thin films by interdiffusion of the PbX$_2$ and MAX precursor stacking layers at 100 °C for 60 min, where the two precursors used are labeled in **Figure 3**b, which shows the absorption spectra of these formed perovskite films. The bandgap tunability of mixed halide perovskites has been widely studied,[16] however, there has not been sufficient evidence for the incorporation of chlorine into the perovskite.[17] In this study, we observed a clear bandgap increase (Figure 3b) for bromide-chloride mixed perovskites, which provides the first experimental evidence that incorporation of Cl could be able to increase the bandgap of perovskite. To confirm the interdiffusion reaction process can be applied to the fabrication of all the trihalide and mixed trihalide perovskite thin films, X-ray Diffraction (XRD) was studied and shown in Figure 3a. All the perovskite thin films have the similar pattern, but it is obvious that each XRD peak has a shift to larger diffraction angle, which indicates that the lattice constant has been reduced by introducing Br to substitute I, and further reduced by introducing Cl to substitute Br. This is reasonable because of the smaller atom size of Cl and Br than I. Another noticeable finding is the distinct strong exciton absorption peaks close

to the absorption cut-off edge for perovskite films containing Br and Cl (Figure 3b). It is noted that such strong excitonic absorption peaks are only observed in organolead trihalide perovskite films formed on flat surface, which might be explained by the lesser screening of rotational organic ions in these films. By measuring the full width at half-maximum of the exciton absorption peaks,[18] we estimated that the exciton binding energies to be 80 meV for MAPbBr$_3$ and 87 meV for MAPbBr$_{3-x}$Cl$_x$, both of which are larger than that of MAPbI$_3$ (19–56 meV). To find out whether these large binding energy excitons can be dissociated and contribute to the photocurrent in Br and Cl based perovskite devices, we measured the wavelength dependent photocurrents of the corresponding devices by IPCE. Figure 3c shows the external quantum efficiency (EQE) curves of the devices based on the four types of perovskite thin films, with the device structure of ITO/PEODT:PSS/MAPbX$_3$/PCBM/C$_{60}$/BCP/Al. The EQE peaks are consistent with the exciton absorption peaks, proving that the excitons generated in mixed halide perovskite could be efficiently dissociated despite the large exciton binding energy over 80 meV.

Since MAPbBr$_3$ has a larger bandgap than C$_{60}$, its absorption and EQE spectrum band can be separated from that of C$_{60}$, both of which allow us to study the electric field dependent exciton dissociation behavior of these two materials in a single device. We expect to see a fundamental difference between excitonic materials and nonexcitonic materials on the electric field dependent charge generation. For nonexcitonic materials, free charges are generated upon light absorption, thus the electric field has no effect on charge generation yield; while for excitonic materials, the excitons with large binding energy need to be dissociated either by a large energy offset at the donor–acceptor interface or by a strong electric field that draws the electron and hole apart. The field-dependent dissociation rate, k_D, can be described quantitatively by the Onsager model[19]

$$k_D(E) = k_R \frac{3}{4\pi a^3} e^{-E_B/kT} \left[1 + b + \frac{b^2}{3} + \frac{b^3}{18} + \frac{b^4}{180} + \cdots \right] \quad (1)$$

where k_R is the bimolecular rate constant of the bound electron–hole pair (e–h pair), a is the initial separation of the bound e–h pair at the interface, $b = e^3 E / 8\pi \varepsilon_0 \varepsilon_r k^2 T^2$, ε_0 is the dielectric permittivity of the vacuum, ε_r is the relative
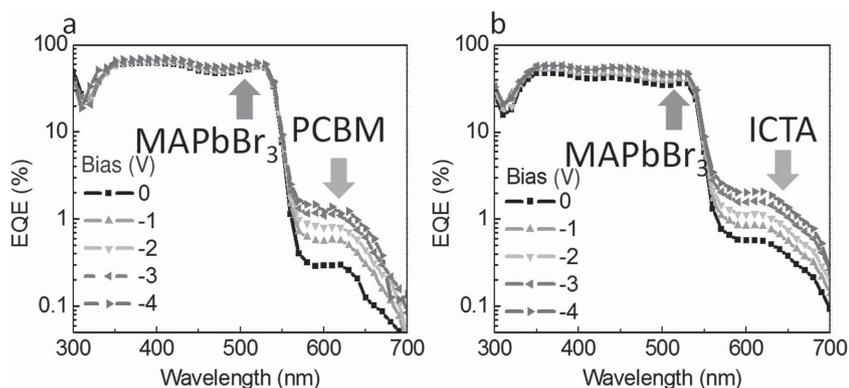
Figure 4. EQE spectra of the MAPbBr3 devices with different electron collection layers of PCBM a) and ICTA b) under the increasing reverse bias from 0 to −4 V; EQE signals between 560 and 700 nm are contributed by fullerenes.

dielectric permittivity of the active layer, and E_B is the e–h pair's binding energy. According to the Onsager model, field-dependent dissociation rate cannot be predicted by materials intrinsic parameters, such as exciton binding energy or dielectric constant exclusively. In order to examine this dynamic property, we continued to test the external electric fields dependent EQE of MAPbBr$_3$ devices with structures of ITO/PEDOT:PSS (30 nm)/MAPbBr$_3$ (100 nm)/PCBM/C$_{60}$ (200 nm)/BCP (80 nm)/Al (100 nm) and ITO/PEDOT:PSS (30 nm)/MAPbBr$_3$ (100 nm)/spun ICTA/ evaporated ICTA (200 nm)/BCP (80 nm)/Al (100 nm). Here there is a possibility that thermal deposited ICTA may decompose into C$_{60}$ and other fragments, however, the spun layer of ICTA stays still on the perovskite thin films during the whole process. Since the LUMO level of ICTA is not lower than that of MAPbBr$_3$ (Figure 2a), the existence of ICTA excludes the situation that the inner electric field offered by the LUMO offset between MAPbBr$_3$ and ICTA could assist the dissociation of photoinduced excitons.

As shown in **Figure 4**a,b, the devices have a reasonably high EQE of around 60% in MAPbBr$_3$'s absorption spectral range at zero bias. While the EQE in the absorption band of 560–750 nm, where only PCBM, C$_{60}$, or ICTA absorbs, is close to zero. This indicates that the photoinduced charge transfer from PCBM, C$_{60}$, or ICTA to MAPbBr$_3$ is negligible, excluding the possibility that band offset exits at MAPbBr$_3$/PCBM or MAPbBr$_3$/ICTA interface. With a gradually increasing external electric field up to 0.8×10^5 V cm^{-1} (4 V applied on approximate 500 nm device), the EQE in the MAPbBr$_3$ absorption band remains unchanged during the whole process, but increases dramatically by 4–5 times in the PCBM, ICTA, or C$_{60}$ absorption band. We infer that the generated excitons in MAPbBr$_3$ have obtained a nearly maximum dissociation efficiency even without an external electric field or an energy level offset at

the heterogeneous interface. However, few excitons generated in PCBM, ICTA, or C$_{60}$ dissociated into free charges to contribute to the photocurrent unless a large reverse bias was applied. The reason is that the absorbed sunlight in the 560–750 nm wavelength range can yield photocurrent only from Frenkel exciton dissociation, since the bandgap of charger transfer excitons (CTEs) in fullerene of ≈2.3 eV is too larger.[20] CTEs are formed by delocalized electrons transfer between the fullerene molecules, which is considered to be responsible to the photocurrent yield from fullerenes based Schottky junction device.[21] This result verified the field independent exciton dissociation in MAPbBr$_3$ and field dependent exciton dissociation in fullerenes, providing another piece of evidence for the non-excitonic nature of MAPbBr$_3$ despite having larger exciton binding energy than MAPbI$_3$.

We also replaced fullerenes in this same device structure by another excitonic material, poly[4,8-bis-(2-ethyl-hexyl-thiophene-5-yl)-benzo[1,2-b:4,5-b']dithiophene-2,6-diyl]-alt-[2-(2'-ethyl-hexanoyl)-thieno[3,4-b]thiophen-4,6-diyl] (PBDTTT-CT), a semiconducting polymer known to form Frenkel type excitons upon light absorption (**Figure 5**a).[22] Again, the large bandgap difference between MAPbBr$_3$ and PBDTTT-CT allows the photocurrent contribution from either material to be distinguished from the other in the single device. Figure 5b shows the results of this device from field dependent EQE test. Notably, there is still a distinct exciton peak at the shoulder of EQE spectra near the MAPbBr$_3$ absorption edge. PBDTTT-CT has been regarded as a hole conduction material, and the energy level for which shows that there is a potential barrier to electron transfer from perovskite to PBDTTT-CT (Figure 2a). So we measured the photocurrent of this device, shown in the inset of Figure 5b, and found that photogenerated electrons could be transported through 110 nm thick PBDTTT-CT and collected by BCP/Al electrode. There is a small increase of EQE in the absorption band of MAPbBr$_3$, which can be explained by
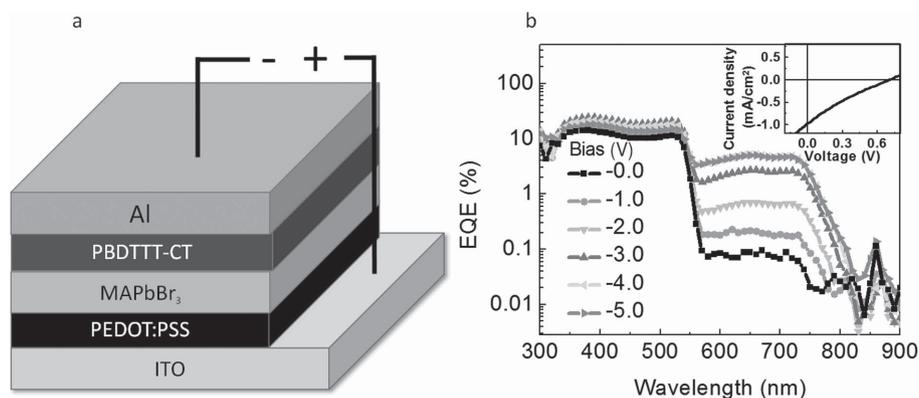

Figure 5. a) Device structure of MAPbBr$_3$ thin film with the electron collection layer of PBDTTT-CT. b) EQE spectra of the device under increasing reverse bias from 0 to −4 V; the inserted plot is photocurrent curve of the device.

the improved collection of electrons generated in MAPbBr$_3$ under reverse bias by overcoming the energy barrier from MAPbBr$_3$ to PBDTTT-CT. The relative EQE height of the MAPbBr$_3$ exciton peak at 520 nm with respect to other wavelength does not change with the increasing reverse bias, suggesting that the exciton dissociation rate is not field dependent in MAPbBr$_3$. The EQE spectra of the device with the perovskite/polymer are subtly different from those of the device with the perovskite/fullerenes as active layer. The EQE from perovskite absorption range is much lower, which is assigned to the energy barrier at the perovskite/polymer interface and to the much worse electron conducting capability of PBDTTT-CT. Compared to the small rise of EQE from MAPbBr$_3$ absorption band, the EQE from PBDTTT-CT absorption band between 550 and 800 nm increases by almost two orders of magnitude. This is the first time such a large electric field dependent Frenkel exciton dissociation was observed.

To summarize, we demonstrated that MAPbI3 is a nonexcitonic material by measuring the dielectric constant, and the V_{OC} variation with respect to the LUMO offset between MAPbI3 and various fullerenes. Then we found that bromine-based perovskites also exhibit a nonexcitonic nature based on the disparate results from the field dependent EQE of perovskite and excitonic semiconductors. We further concluded that even though MAPbBr3 or mixed halide perovskite have relatively large exciton binding energy in excess of 80 meV, they still should be treated as nonexcitonic semiconductors. The nonexcitonic nature of perovskites enables an efficient free charge generation, which explains the outstanding performance of perovskite solar cells.

Experimental Section

Sample Preparation: The organometal trihalide perovskite thin films were prepared by the interdiffusion of spin coated stacking layers of methylammonium halide (MAI, MACl, MABr) and lead halide (PbI$_2$, PbBr$_2$) solutions. Methylammonium halide precursor were synthesized using the methods described in previous study by Lee et al.[3] PbI$_2$ and PbBr$_2$ precursors were dissolved in anhydrous N,N-dimethylformamide (DMF) with concentration of 400 mg mL^{-1} and 300 mg mL^{-1}, respectively. Methylammonium halide precursors were formed by dissolving MAI, MACl, and MABr into 2-propanol with concentration of 35, 28.6, and 20 mg mL^{-1}, respectively. The PbBr$_2$ solution was spun on PEDOT:PSS substrate at 70 °C at 6 000 rounds/s (rpm) for 35 s. Then methylammonium halide solutions were spun on top of dried PbI$_2$ or PbBr$_2$ film at 6 000 rpm for 35 s at room temperature. The spin coated PbI$_2$/MAI and PbBr$_2$/MAI or MACl or MABr stacking films were solvent annealed at 100 °C for 90 min.[23]

The MAPbI$_3$ layer in the device for impedance study was fabricated by the similar interdiffusion routine, but with higher concentration precursors as 900 mg mL^{-1} PbI$_2$ and 105 mg mL^{-1} MAI solutions, which resulted the thickness of MAPbI$_3$ to be 1000 nm. The device was finished by thermal evaporating of Au (30 nm)/Ag (70 nm) electrodes on the nude MAPbI$_3$ thin film. Excitonic materials, including, PCBM/C$_{60}$, ICTA, PBDTTT-CT, were spun directly on MAPbX thin films at 6000 rpm for 35 s from their

1,2-dichlorobenzene (DCB) solutions (2% wt). PCBM and ICTA were thermal annealed for 1 h, while the samples with PBDTTT-CT were fast dried on 70 °C oven for 5 min. The devices with fullerenes were finished by the subsequent thermal evaporating either 20 nm C$_{60}$ on PCBM or 20 nm ICTA on spun ICTA, and BCP (8 nm) and Al (100 nm). The device with PBDTTT-CT was finished by thermal evaporating BCP (8 nm) and Al (100 nm). The device area is defined to be the overlap of the ITO and aluminum electrodes to be 9.6 mm^2.

Film and Device Characterization: The frequency dependent relative dielectric constant of MAPbI$_3$ was evaluated by E4980A over a wide range of 20 Hz to 20 MHz in the dark condition and zero bias. A Quanta 200 FEG Environmental Scanning Electron Microscope (ESEM) using a field-emission gun (FEG) electron source was used to scan the film morphology. The films were first covered with a thin layer of gold coated using a Cressington 108 Auto Sputter Coater before the SEM measurement. Absorption spectra were recorded by Evolution 201 UV-Visible Spectrophotometer. XRD measurements were performed with a Rigaku D/Max-B X-ray diffractometer with Bragg–Brentano parafocusing geometry, a diffracted beam monochromator, and a conventional copper target X-ray tube set to 40 kV and 30 mA. The photocurrents were measured using a xenon-lamp-based solar simulator (Oriel 67005). A Schott visible-color glass-filtered (KG5 color-filtered) Si diode (Hamamatsu S1133) was used to calibrate the light intensity before photocurrent measurement. EQE was measured with a Newport QE measurement kit by focusing a monochromatic beam of light onto the devices.

[1] H.-S. Kim, C.-R. Lee, J.-H. Im, K.-B. Lee, T. Moehl, A. Marchioro, S.-J. Moon, R. Humphry-Baker, J.-H. Yum, J. E. Moser, M. Grätzel, N.-G. G. Park, *Sci. Rep.* **2012**, *2*, 591.

[2] L. Etgar, P. Gao, Z. Xue, Q. Peng, A. K. Chandiran, B. Liu, M. K. Nazeeruddin, M. Grätzel, *J. Am. Chem. Soc.* **2012**, *134*, 17396.

[3] M. M. Lee, J. Teuscher, T. Miyasaka, T. N. Murakami, H. J. Snaith, *Science* **2012**, *338*, 643.

[4] Z. Xiao, C. Bi, Y. Shao, Q. Dong, Q. Wang, Y. Yuan, C. Wang, Y. Gao, J. Huang, *Energy Environ. Sci.* **2014**, *7*, 2619.

[5] a) T. Ishihara, *J. Lumin.* **1994**, *60*, 269; b) K. Tanaka, T. Takahashi, T. Ban, T. Kondo, K. Uchida, N. Miura, *Solid State Commun.* **2003**, *127*, 619; c) S. Sun, T. Salim, N. Mathews, M. Duchamp, C. Boothroyd, G. Xing, T. C. Sum, Y. M. Lam, *Energy Environ. Sci.* **2014**, *7*, 399.

[6] N. C. Giebink, G. P. Wiederrecht, M. R. Wasielewski, S. R. Forrest, *Phys. Rev. B* **2011**, *83*, 195326.

[7] H.-S. Kim, I. Mora-Sero, V. Gonzalez-Pedro, F. Fabregat-Santiago, E. J. Juarez-Perez, N.-G. Park, J. Bisquert, *Nat. Commun.* **2013**, *4*, 2242.

[8] V. D'Innocenzo, G. Grancini, M. J. Alcocer, A. R. Kandada, S. D. Stranks, M. M. Lee, G. Lanzani, H. J. Snaith, A. Petrozza, *Nat. Commun.* **2013**, *5*, 3586.

[9] E. J. J-Perez, R. S. Sanchez, L. Badia, G. G-Belmonte, Y. Kang, I. M-Sero, J. Bisquert, *J. Phys. Chem. Lett.* **2014**, *5*, 2390.

[10] A. Poglitsch, D. Weber, *J. Chem. Phys.* **1987**, *87*, 6373.

[11] J. Y. Jeng, Y. F. Chiang, M. H. Lee, S. R. Peng, T. F. Guo, P. Chen, T. C. Wen, *Adv. Mater.* **2013**, *25*, 3727.

[12] Q. Wang, Y. Shao, Q. Dong, Z. Xiao, Y. Yuan, J. Huang, *Energy Environ. Sci.* **2014**, *7*, 2359.

[13] a) M. K. Alam, Y. T. Yeow, *Appl. Phys. Lett.* **1980**, *37*, 469; b) K. Vandewal, K. Tvingstedt, A. Gadisa, O. Inganäs, J. V. Manca, *Nat. Mater.* **2009**, *8*, 904.

[14] J. Shi, J. Dong, S. Lv, Y. Xu, L. Zhu, J. Xiao, X. Xu, H. Wu, D. Li, Y. Luo, *Appl. Phys. Lett.* **2014**, *104*, 063901.

[15] Y. Shao, Z. Xiao, C. Bi, Y. Yuan, J. Huang, *Nat. Commun.* **2014**, *5,* 5784.

[16] a) N. J. Hong, I. S. Hyuk, H. J. Hyuck, N. M. Tarak, S. Sang Il, *Nano Lett.* **2013**, *13*, 1764; b) B. Suarez, V. Gonzalez-Pedro, T. S. Ripolles, R. S. Sanchez, L. Otero, I. Mora-Sero, *J. Phys. Chem. Lett.* **2014**, *5*, 1628; c) G. Xing, N. Mathews, S. S. Lim, N. Yantara, X. Liu, D. Sabba, M. Grätzel, S. Mhaisalkar, T. C. Sum, *Nat. Mater.* **2014**, *13*, 476.

[17] a) E. Edri, S. Kirmayer, M. Kulbak, G. Hodes, D. Cahen, *J. Phys. Chem. Lett.* **2014**, *5*, 429; b) S. Colella, E. Mosconi, P. Fedeli, A. Listorti, F. Gazza, F. Orlandi, P. Ferro, T. Besagni, A. Rizzo, G. Calestani, G. Gigli, F. De Angelis, R. Mosca, *Chem. Mater.* **2013**, *25*, 4613.

[18] D. Moses, J. Wang, A. J. Heeger, N. Kirova, S. Brazovski, *Proc. Natl. Acad. Sci. U.S.A.* **2001**, *98*, 13496.

[19] a) L. B. Charles, *J. Chem. Phys.* **1984**, *80*, 4157; b) D. Veldman, O. Ipek, S. C. Meskers, J. Sweelssen, M. M. Koetse, S. C. Veenstra, J. M. Kroon, S. S. van Bavel, J. Loos, R. A. Janssen, *J. Am. Chem. Soc.* **2008**, *130*, 7721; c) T. J. R. Y. Yuan, P. Sharma, S. Poddar, S. Ducharme, A. Gruverman, Y. Yang, J. Huang, *Nat. Mater.* **2011**, *10*, 296.

[20] a) B. Yang, F. Guo, Y. Yuan, Z. Xiao, Y. Lu, Q. Dong, J. Huang, *Adv. Mater.* **2013**, *25*, 572; b) C. Steffan, O. Hideo, K. Youngkyoo, J. B.-S. Jessica, D. C. B. Donal, R. D. James, *Chem. Phys. Lett.* **2007**, *445*, 276.

[21] R. Munn, P. Barbara, P. Piotr, *Phys. Rev. B* **1998**,*57*,1328; b) J. Jacek, I. Stephan, G. S. Bobby, M. Keiji, *J. Phys. Chem. Lett.* **2012**, *11*, 1536.

[22] a) G. Schwartz, M. Pfeiffer, S. Reineke, K. Walzer, K. Leo, *Adv. Mater.* **2007**, *19*, 3672; b) X. Li, W. C. Choy, L. Huo, F. Xie, W. E. Sha, B. Ding, X. Guo, Y. Li, J. Hou, J. You, *Adv. Mater.* **2012**, *24*, 3046; c) L. Dou, J. You, Z. Hong, Z. Xu, G. Li, R. A. Street, Y. Yang, *Adv. Mater.* **2013**, *25*, 6642.

[23] a) J. N. Joong, N. J. Hong, K. Y. Chan, Y. W. Seok, R. Seungchan, S. S. Il, *Nat. Mater.* **2014**, *13*, 897; b) Z. Xiao, Q. Dong, C. Bi, Y. Shao, Y. Yuan, J. Huang, *Adv. Mater.* **2014**, *26*, 6503.